

Proteomic comparison defines novel markers to characterize heterogeneous populations of extracellular vesicle subtypes

Joanna Kowal^a, Guillaume Arras^b, Marina Colombo^a, Mabel Jouve^a, Jakob Paul Morath^a, Bjarke Primdal-Bengtson^a, Florent Dingli^b, Damarys Loew^b, Mercedes Tkach^a, and Clotilde Théry^{a,1}

^aInstitut Curie, PSL Research University, INSERM U932, Department "Immunité et Cancer", 75248 Paris, France; and ^bInstitut Curie, PSL Research University, Centre de Recherche, Laboratoire de Spectrométrie de masse Protéomique, 75248 Paris, France

Edited by Randy Schekman, University of California, Berkeley, CA, and approved January 5, 2016 (received for review October 28, 2015)

Extracellular vesicles (EVs) have become the focus of rising interest because of their numerous functions in physiology and pathology. Cells release heterogeneous vesicles of different sizes and intracellular origins, including small EVs formed inside endosomal compartments (i.e., exosomes) and EVs of various sizes budding from the plasma membrane. Specific markers for the analysis and isolation of different EV populations are missing, imposing important limitations to understanding EV functions. Here, EVs from human dendritic cells were first separated by their sedimentation speed, and then either by their behavior upon upward floatation into iodixanol gradients or by immuno-isolation. Extensive quantitative proteomic analysis allowing comparison of the isolated populations showed that several classically used exosome markers, like major histocompatibility complex, flotillin, and heat-shock 70-kDa proteins, are similarly present in all EVs. We identified proteins specifically enriched in small EVs, and define a set of five protein categories displaying different relative abundance in distinct EV populations. We demonstrate the presence of exosomal and nonexosomal subpopulations within small EVs, and propose their differential separation by immuno-isolation using either CD63, CD81, or CD9. Our work thus provides guidelines to define subtypes of EVs for future functional studies.

exosomes | microvesicles | ectosomes | dendritic cells | extracellular vesicles

In the last decade communication between cells via secretion of membrane vesicles (collectively called extracellular vesicles or EVs) has become the focus of increasing interest (reviewed in refs. 1–3). EVs are composed of a lipid bilayer containing transmembrane proteins and enclosing soluble proteins and RNA. The communication via EVs might be mediated by their multiple components. The surface receptors of EVs allow their targeting and capture by recipient cells, which can then incorporate proteic, lipidic, and even genetic messages carried by the vesicles, resulting in modifications of their physiological state (1, 4, 5). Consequently, the possibility of using these vesicles as biomarkers in various diseases, as vehicles of immunotherapies, or as targets to be eliminated to improve patients' health is currently being explored (2, 6).

It has become clear, however, in the past few years, that cells can release EVs of different types. Some EVs are directly formed and released from the cells' plasma membrane (PM), and are often called microparticles, (shed) microvesicles, or ectosomes: these EVs display sizes ranging from a few dozens of nanometers to a few micrometers. Internal vesicles generated within multivesicular endosomal compartments (MVB) are secreted when these compartments fuse with the PM, thus releasing their internal vesicles in the extracellular milieu: these EVs are termed exosomes (3, 7). Exosomes are classically defined by their size, similar to the size of intraluminal vesicles of MVBs (i.e., below 150 nm in diameter), and their content of endosome-associated proteins. However, the term exosome is often used in the literature for EVs of small size, passing through 220-nm pore filters

or recovered by high-speed ultracentrifugation (8), in the absence of demonstration of their intracellular origin. Such isolation procedures coisolate mixed EV populations, which we will call "small EVs" (sEVs), for lack of better term, in the rest of this article. Because EVs of different intracellular origins probably have different functional properties (9, 10), the mixed nature of EV preparations has made the growing literature increasingly confusing, with contradictory proposed functions and clinical uses of vesicles being regularly published. The lack of specific purification and characterization tools prevents a clear understanding of the specific versus shared functional properties of the different EVs. There is, therefore, a critical need for the identification of specific markers defining the different subtypes of EVs.

To achieve this goal, we have performed here an extensive comparative analysis of the protein composition of all EVs recovered in the different steps of the differential ultracentrifugation (DUC) protocol classically used to isolate sEVs (11). As a source of EVs, we used human primary monocyte-derived dendritic cells (DCs), whose exosomes and EVs have been described to promote immune responses (1, 12).

We found that several proteins often used in the literature as "exosome-markers," such as flotillin-1, heat-shock 70-kDa proteins (HSC70/HSP73, HSP70/HSP72), or major histocompatibility complex (MHC) class I and class II proteins are present, to

Significance

The last decade has seen a rapid expansion of interest in extracellular vesicles (EVs), proposed to mediate cell–cell communication in patho/physiological conditions. Although heterogeneity of EVs has become obvious, as highlighted recently by the International Society for Extracellular Vesicles, the field is lacking specific tools to distinguish EVs of different intracellular origins, and thus probably different functions. Here, thanks to a comprehensive comparison of different types of EVs isolated from a single cell type, we define proteins generically present in EVs, small EV-specific and -excluded ones, and a few specific of endosome-derived exosomes or non-exosomal small EVs. This work will allow proper evaluation of the molecular mechanisms of biogenesis and secretion and the respective functions of subtypes of EVs.

Author contributions: J.K., D.L., M.T., and C.T. designed research; J.K., M.C., M.J., J.P.M., B.P.-B., and F.D. performed research; J.K., G.A., M.C., M.J., J.P.M., F.D., M.T., and C.T. analyzed data; and J.K., M.T., and C.T. wrote the paper.

The authors declare no conflict of interest.

This article is a PNAS Direct Submission.

Data deposition: Raw proteomic data have been deposited in the ProteomeXchange Consortium (www.proteomexchange.org) via the PRIDE partner repository (accession no. PXD003257).

¹To whom correspondence should be addressed. Email: clotilde.thery@curie.fr.

This article contains supporting information online at www.pnas.org/lookup/suppl/doi:10.1073/pnas.1521230113/-DCSupplemental.

various extents, not only in the sEVs pelleted at high speed, but also in the larger/heavier EVs pelleted at medium or low speed. We further separated the pelleted EVs by floatation into a density gradient or by immuno-isolation with antibodies specific for the three tetraspanins classically used as exosome markers (CD9, CD63, CD81), and performed a label-free quantitative proteomic analysis of their respective composition. We thus identified more specific protein markers of either the sEVs, among which a subpopulation bearing all tetraspanins correspond to endosome-derived exosomes, or the larger/heavier vesicles.

Results

Primary DCs Secrete EVs of Different Sizes. We here analyzed EVs secreted by human primary monocyte-derived DCs. Heterogeneity in size of EVs recovered by DUC from these cells (13), and the presence of membrane-enclosed structures at the DC surface (Fig. 1A) suggest that they may actively secrete EVs of different intracellular origins. Conditioned medium was collected from DCs after 24-h incubation in medium depleted from FCS-derived EVs, and subjected to DUC, as previously described (11). Pelleted materials recovered by low (2,000 × g = 2K) or medium (10,000 × g = 10K) centrifugation speed were washed and compared with the ultracentrifugation pellet (100,000 × g = 100K), classically considered as containing exosomes (Fig. 1B). The total amount of proteins pelleted at low speed (2K) was significantly higher than the amount pelleted at 10K or 100K (Fig. 1C). In these culture conditions, less than 10% cell death was generally observed, and the amount of material recovered in the 2K pellet did not positively correlate with cell death (Fig. S1A), showing that these large EVs are not apoptotic/necrotic cell fragments. When analyzed by transmission electron microscopy (TEM), whole-mounts of materials recovered in the 2K pellet showed vesicles in majority larger than 150 nm in diameter (Fig. 1D and E). In contrast, a majority of vesicles pelleting at 10K and at 100K were of the size generally described for exosomes (i.e., 50–150 nm), about 10% of the remaining EVs being smaller than 50 nm (Fig. 1D and E). Nanoparticle tracking analysis confirmed the higher representation of large vesicles in the 10K pellet, resulting in a mean size above 200 nm for the 10K, and below 200 nm for the 100K pellet (Fig. S1B). The total number of particles secreted per cell was slightly smaller in the 10K than 100K pellet (Fig. S1B). Thus, live human primary DCs release a large range of EVs, which are partially separated by their pelleting properties.

Classic Exosome Markers Are also Detected in Other EVs. A few protein markers are often used in the literature to characterize exosomes in mixed sEV populations. We thus compared here their distribution among the other EVs, by analyzing on Western blots the same amount of proteins from each centrifugation pellet or from the secreting cell lysates (Fig. 1F; quantifications of three to nine independent experiments shown in Fig. S1C). As expected, tetraspanins (CD9, CD63, CD81) were highly abundant in the 100K pellet containing exosomes, but CD63 and CD9 were also present, although to various degrees, in the 2K and the 10K pellets. On the other hand, flotillin-1 (*FLOT1*), the constitutive heat-shock protein HSC70 (*HSPA8*), MHC class II (*HLA-DRA*) and actin, as well as MHC class I (*HLA-A/B/C/G*) and HSP70 (*HSP1A1*) (Fig. S1D) were not enriched in the 100K pellets compared with the levels in other pellets, and thus could not be considered as sEV- (nor exosome-) specific markers. The exosome-excluded endoplasmic reticulum (ER) protein GP96, also called GRP94 or endoplasmic reticulum chaperone (*HSP90B1*), was hardly detectable in both the 10K and 100K pellets, but abundant in the 2K pellet and the whole cells (Fig. 1F), suggesting that large EVs contain various parts of the secreting cell.

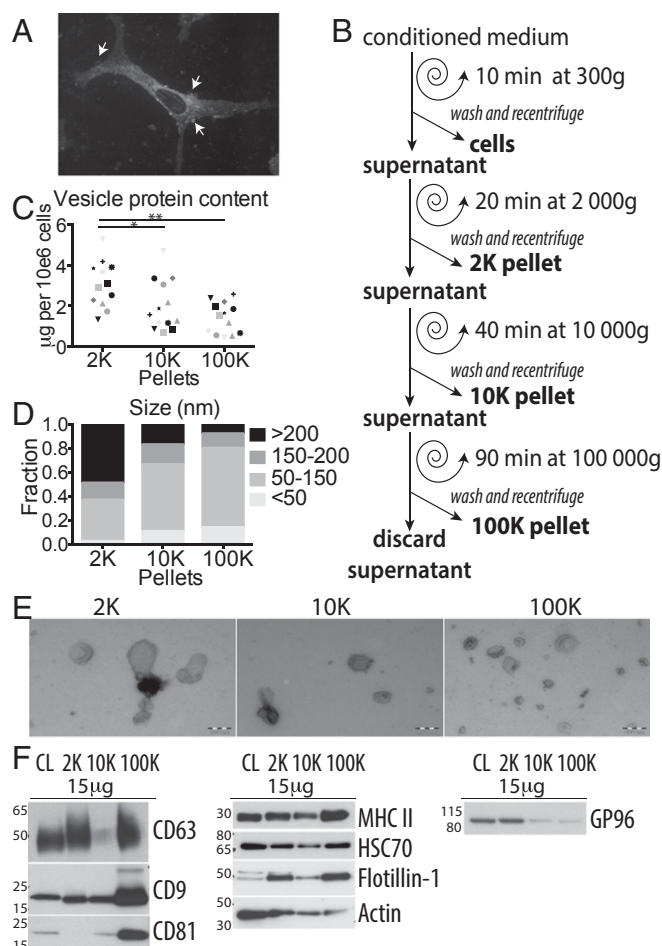


Fig. 1. DCs secrete heterogeneous EVs recovered in successive differential ultracentrifugation pellets. (A) DC stained with FM 4-64 FX dye and visualized with confocal microscopy. (Magnification, 100×.) Arrows point at vesicles budding at the cell surface. (B) Scheme of EV isolation by DUC from conditioned medium of human monocyte-derived DCs. (C) Protein content of each pellet (2K = 2,000 × g; 10K = 10,000 × g; 100K = 100,000 × g) is represented for individual donors (one symbol per donor), **P* < 0.05; ***P* < 0.01 (Wilcoxon signed-rank test). (D and E) Whole-mount EM analysis of each pellet showing representative images (E) and size distribution (D) of the vesicles. Diameter of membrane-enclosed structures was determined with iTEM software, for two independent donors (2K *n* = 35 EVs, 10K *n* = 72, 100K *n* = 135). (Scale bars, 200 nm.) (F) The successive pellets (2K, 10K, 100K) of EVs isolated from DCs were analyzed by Western blot side-by-side with the lysate of producing cells (CL), using antibodies to proteins often considered as “exosome-markers.” Equivalent protein amounts of each sample were loaded on the gels. Representative images and quantifications in three to nine individual donors (Fig. S1C) are shown. As expected for sEV-markers, tetraspanins (CD63, CD9, CD81) are enriched in 100K, but CD9 and CD63 are also abundant in the 10K and 2K pellets respectively. Other putative sEVs markers (MHC II, HSC70, flotillin-1, actin) are ubiquitously present in the three pellets. The ER-retained protein GP96 is mainly found in cells and the material pelleting at the lowest speed, 2K.

Floatation into Iodixanol or Sucrose Gradients Differently Separates Subtypes of EVs. Because most of the above proteins were not specific for a given type of DUC-isolated EV, our next goal was to set up another separation assay. Density gradients, either of sucrose or iodixanol, are a classic means to separate membrane-enclosed vesicles according to their floatation speed and equilibrium density (2). We first used a self-forming iodixanol (=OptiPrep) gradient to subfractionate the 10K and 100K pellets. These pellets were resuspended in Tris buffer containing 30% (wt/vol) iodixanol, and allowed to float into an overlaid gradient during a short (1 h) ultracentrifugation (Fig. 2A). Overlaying the

gradient on top of the EV pellet ensured that membrane-enclosed vesicles floated upwards, whereas protein aggregates could not float into the gradient and remained in the dense fractions (14, 15). Ten fractions were recovered and analyzed for the presence of protein markers previously detected in both pellets. As shown in Fig. 2B, materials recovered after either 10K or 100K centrifugation floated mostly in two discrete fractions of, respectively, on average 1.115 g/mL (third fraction = F3) and 1.145 g/mL (fifth fraction = F5) of iodixanol. These four different fractions all contained vesicles bearing MHC class II, but also tetraspanins (CD9 and CD63), although CD63 was not very abundant in the dense fraction from the 100K pellet (so-called F5-100K). Each fraction was analyzed as whole-mounts by TEM (Fig. 2C): the F3-100K pellet contained a vast majority of vesicles of 50–150 nm in diameter, whereas all of the other fractions contained

larger vesicles as well, sometimes with dense cores. Thus, floatation into iodixanol gradients allows separation of subtypes of EVs displaying different buoyant densities and sizes, with sEVs strongly enriched in the light fraction of the high-speed ultracentrifugation pellet (F3-100K).

In contrast, floatation of the 10K and 100K pellets into overlaid sucrose led to a continuum of fractions containing MHC class II and tetraspanins, ranging from densities of 1.12–1.19 g/mL for the 100K pellet, and 1.12–1.21 g/mL for the 10K pellet (Fig. 2D), corresponding to the density range classically assigned to sEVs [1.13–1.19 g/mL (2)]. The majority of EVs floated at 1.15 g/mL for the 100K pellet and at 1.17 g/mL for the 10K pellet: that is, at different densities but in adjacent fractions, which did not allow accurate separation for further analysis. The difference in separation of vesicles in sucrose versus iodixanol

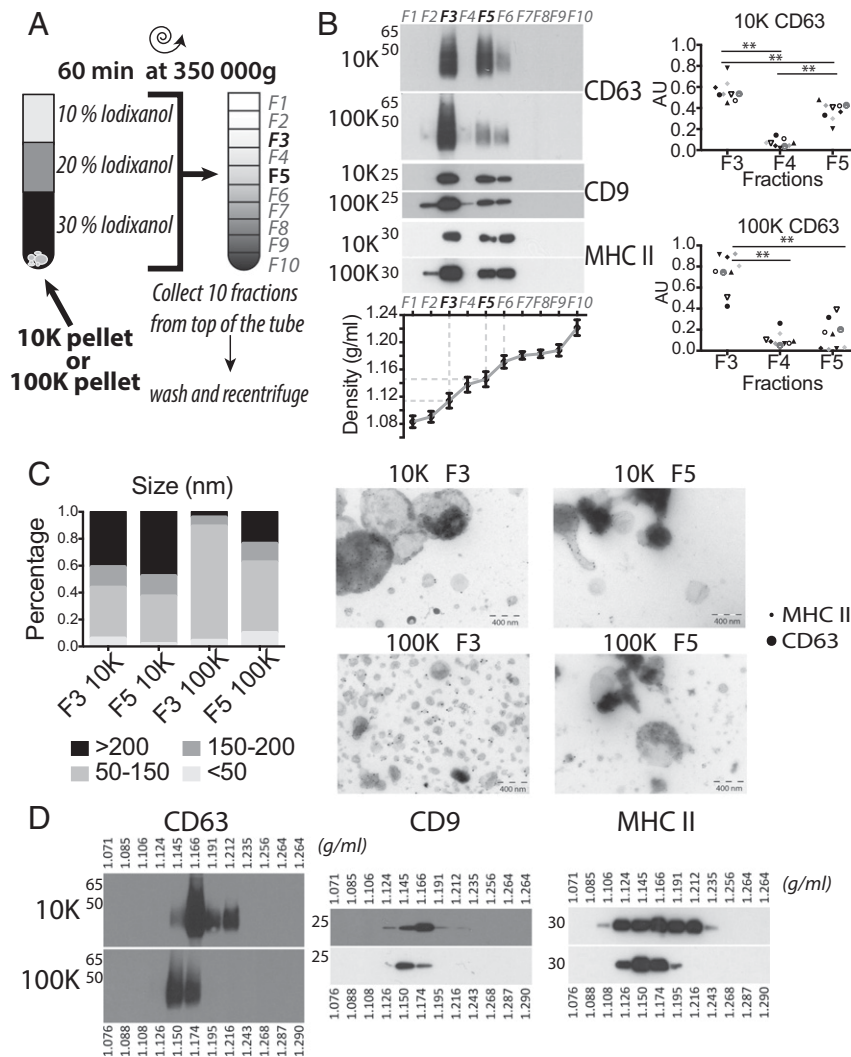


Fig. 2. Floatation on iodixanol gradient separates four subfractions of EVs. (A) Pellets obtained after 10K and 100K centrifugations were allowed to float into an overlaid iodixanol gradient. (B) Ten fractions were collected and analyzed by Western blot (representative of nine experiments), showing the separation of two discrete fractions (F3 and F5+F6) of EVs from both the 10K and 100K pellets (Left). Densities of recovered fractions, as measured by refractometry, are displayed in the graph (mean \pm SD of 36 independent gradients). (Right) Quantification of CD63 relative abundance in fractions F3–F5 of both pellets obtained from nine individual donors was performed as in Fig. S1C. Arbitrary Units (AU) = $(SI_{fraction}) / \text{Sum}(SI_{F3} + SI_{F4} + SI_{F5})$ where SI = signal intensity. Each symbol represents a single donor. $**P < 0.01$ (Wilcoxon signed-rank test). (C) Representative images of whole-mount EM of fractions three and five of 10K and 100K (Right), and size distribution of vesicles measured by ImageJ software (Left: F3 10K $n = 98$, F5 10K $n = 99$, F3100K $n = 226$, F5 100K $n = 166$, representative of two independent gradients). (Scale bar, 400 nm.) (D) Separation of 10K and 100K pellets on sucrose gradients analyzed by Western blot shows continuous distribution between 1.12 and 1.19 g/mL for both pellets, and a tendency for 10K to achieve equilibrium in denser fractions (1.17 and above) than 100K (1.15 + 1.17).

could be a result of differences in the osmotic pressure of these two gradients (16), potentially affecting the EVs.

Quantitative Proteomic Analysis of Four Fractions of EVs Obtained upon Iodixanol Floatation. Extensive proteomic analysis was then performed simultaneously on the four individual fractions recovered from iodixanol gradient floatation of the 10K and the 100K pellet (i.e., F3-10K, F5-10K, F3-100K, F5-100K) from three biological replicates, and the respective amount of identified proteins in these different samples was quantified by a label-free approach. Qualitative analysis, evaluating the presence of proteins identified by at least three distinct peptides, showed that the majority of proteins were common to several fractions, but also that each fraction contained a restricted set of unique proteins (Fig. 3A, Table S1, and Dataset S1). Gene Ontology (GO) term enrichment analysis of these unique proteins showed specific accumulation of ribosome proteins in both F3 and F5 fractions of the 10K pellet, of both mitochondrial and ER proteins in F5-10K, and of proteasome proteins in F3-10K. In the 100K pellet, extracellular matrix proteins (ECM) were specifically present in the F5 fraction (e.g., collagen, *COL6A3*; PEDF, *SERPINF1*) (Table S1), whereas PM and endosomal proteins were accumulated in the light fraction (F3).

Because most proteins were common to all fractions, we then performed a quantitative comparison of their respective amount in the different fractions compared with F3-100K (Dataset S2).

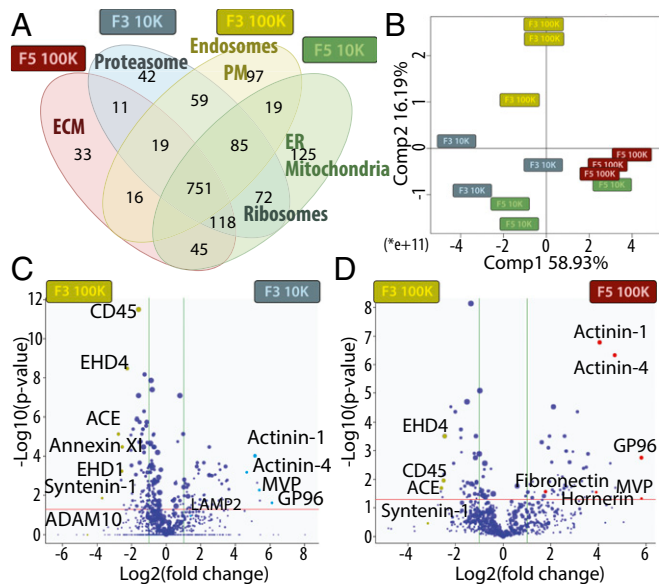


Fig. 3. Qualitative and quantitative proteomic analyses of iodixanol fractions F3 and F5 from 10K and 100K pellets by LC-MS/MS suggest different intracellular origins of the four types of EVs, and identify potential specific proteins. (A) Venn diagram showing the distribution of proteins qualitatively identified in each fraction by at least three peptides in one of the three biological replicates. GO terms of protein families specifically enriched in a single fraction (or in two fractions for ribosomes), as determined by DAVID software, are shown. (B–D) Quantitative analysis of the amount of proteins in each fraction compared with F3-100K was performed (proteins displaying missing values among fractions were excluded from this analysis). (B) PCA analysis of the quantitative comparison shows a clear separation of fraction F3-100K from the three others. (C and D) Quantitative analysis of proteins present in F3-10K (C) or F5-100K (D) compared with F3-100K is shown as Volcano plot. x axis = $\log_2(\text{fold-change})$ (10K/100K), y axis = $-\log_{10}(P \text{ value})$. The horizontal red line indicates $P \text{ value} = 0.05$, vertical green lines indicate absolute fold-change = 2. Data represent results of three independent sets of donors pooled together. Position of proteins selected as potential specific markers of each fraction and analyzed further is shown.

Principal component analysis (PCA) of these quantitative comparisons (Fig. 3B) showed a clear separation of F3-100K from the other three fractions, especially from F5-100K. GO term classification of proteins more abundant in F5-100K compared with F3-100K highlighted extracellular space, and mitochondrial and ribosome components, whereas, conversely, F3-100K was enriched in proteins found in the PM and endosome (Fig. S2, Left). This enrichment in endosomal and PM components in F3-100K was also observed compared with F3-10K, which, in contrast, contained more mitochondrial components (Fig. S2, Right).

Volcano plot representation of the relative abundance in F3-100K and F3-10K (Fig. 3C) identified a few proteins significantly ($P < 0.05$) or more than fourfold enriched in F3-100K: for example, Annexin XI (*ANXA11*), EH domain-containing proteins 1 and 4 (*EHD1*, *EHD4*), angiotensin-converting enzyme (*ACE*), syntenin-1 (*SDCBP*), and “a disintegrin and metalloproteinase domain-containing protein 10” (*ADAM10*). On the other hand, actinins 1 and 4 (*ACTN1* and *ACTN4*), major vault protein (*MVP*), and endoplasmic GP96 (*HSP90B1*) were over fourfold enriched in F3-10K (Fig. 3C). Similar comparison of F3-100K with F5-100K (Fig. 3D) also showed enrichment of actinins, GP96 and MVP, in F5-100K, and highlighted a few proteins specifically enriched in the F5-100K but not the F3-10K fractions (Dataset S2): ECM proteins like fibronectin (*FN1*) and hornerin (*HRNR*), serum-derived proteins such as prothrombin (*F2*), pigment epithelium derived factor (*PEDF* or *SERPINF1*), and complement (*C3*, *C4A*) (Table S1).

Thus, extensive and quantitative proteomic analysis of EVs separated by DUC followed by iodixanol gradient demonstrates the presence of vesicles with different protein content as well as physical properties.

Identification of Specific Markers of Either Large or Small EVs. We next asked whether our comparative proteomic analysis could allow identifying specific markers of the sEVs, or of the large PM-derived EVs. Among the proteins uniquely present (Table S1), or either highly or significantly enriched (Fig. 3C and D) in F3-100K, we selected tumor susceptibility 101 (*TSG101*), syntenin-1, EHD4, Annexin XI, and ADAM10. Conversely, unique or enriched proteins in the other fractions included actinin-4 and mitofilin. We confirmed specific enrichment in F3-100K of the first two proteins (Fig. 4A). When differential centrifugation pellets were analyzed as in Fig. 1 for presence of these markers, we observed a very striking enrichment of syntenin-1, EHD4, and ADAM10 in the 100K pellet, as compared both to the other pellets and to the secreting cells (Fig. 4B; quantifications of three to five independent experiments shown in Fig. S3A), and of TSG101 and Annexin XI compared with the other pellets (but not to the secreting cells), suggesting that these proteins are more specific markers of the sEVs than the commonly used CD63 and CD9 tetraspanins (compare Figs. 1F and 4B). In contrast, Annexin II, which was less than twofold enriched in F3-100K (Dataset S2), was strongly detected by Western blot in both the 10K and 100K pellets (Fig. 4C and Fig. S3A). On the other hand, actinin-4 and mitofilin qualified as markers of the large- and medium-sized EVs, because both were highly abundant in the 2K and 10K pellets and not in the 100K pellet (Fig. 4C and Fig. S3A), whereas lysosomal-associated membrane protein 2 (*LAMP2*; enriched twofold in F3-10K) (Fig. 4C and Dataset S2) and GP96 (Fig. 1F) were similarly detected at low levels or similarly absent in 10K and 100K pellets, hence not discriminant markers of the intermediate-sized EVs.

Distribution of the New Markers on EVs Secreted by Other Cell Types. To determine whether the newly identified set of proteins could also be used to characterize EVs secreted by other cells, we analyzed EV secretion by several human cell lines: five tumoral [OV2008 and MDA-MB-231 (Fig. 4D), IGROV-1, SHIN-3, and

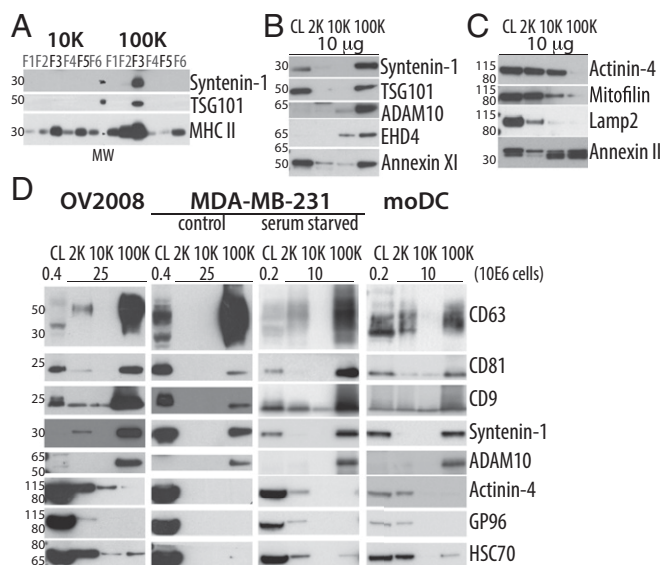


Fig. 4. Confirmation of selected proteins as specific markers of distinct vesicles subpopulation. (A) Western blotting of iodixanol fractions of 10K and 100K confirms the unique presence of TSG101 and syntenin-1 in fraction F3-100K. MW, molecular weight markers. (B and C) Western blot analysis, performed as in Fig. 1F, of the distribution, among the successive pellets of differential centrifugation (2K, 10K, 100K), of selected proteins identified by the quantitative proteomic analysis. Representative images are shown and, quantifications in two to five experiments are displayed in Fig. S3A. As expected from their enrichment in F3-100K, syntenin-1, TSG101, ADAM10, EHD4, and Annexin XI are strongly enriched in 100K and almost absent in the other pellets (B). Conversely, as expected from their enrichment in F3-10K, actinin-4, and mitofilin are enriched in 10K compared with 100K, but they are also present in 2K (C). Proteins which were less than twofold enriched in either fraction, such as LAMP2 or Annexin II did not show, upon Western blotting, differential expression in 10K vs. 100K pellets (C). (D) Western blot analysis of the secretion of various proteins in the different centrifugation pellets recovered from conditioned medium of tumor cell lines OV2008, MDA-MB-231 (in control or serum-starved conditions), compared with DCs. The 2K, 10K, and 100K pellets obtained from the same number of cells were loaded on the gel, side-by-side with CL from the indicated number of cells. Presence of syntenin-1 and ADAM10 and enrichment of CD9/CD63/CD81 was confirmed among all cell lines in 100K pellets. Presence of CD9, CD63, actinin-4 and HSC70 was confirmed in the 2K pellets of cell lines secreting large EVs [i.e., OV2008 and MDA-MB-231 under starvation (no serum) conditions].

HeLa cells (Fig. S3B)] and two immortalized nontumor cell lines [HEK293T and RPE-1 (Fig. S3B)]. Because these cell lines released fewer EVs than human primary DCs, especially in the 2K pellet, materials recovered from a given number of secreting cells (rather than equal protein amounts) were loaded for Western blot analysis. In all these cell lines, sEVs (100K pellet) contained the proteins most enriched in the corresponding DC-derived pellet (syntenin-1, ADAM10, and CD81), as well as CD63 and CD9, and were devoid of the proteins enriched in other EVs (actinin-4, GP96). Most cell lines released very little material pelleting at 2K or 10K, except the ovarian carcinoma OV2008, in which both low- and medium-speed pellets contained, like in DCs, actinin-4, HSC70, and some CD9 and CD63 (Fig. 4D). These molecules could also be detected in the 2K pellets recovered from MDA-MB-231 exposed to starvation, which induces secretion of large EVs, as described by others (17) and confirmed in our hands (shown by SYPRO orange-staining of the gel) (Fig. S3C). Like in human monocyte-derived DCs, we observed in mouse bone marrow-derived DCs the secretion of a wide-range of EVs and similar behavior of the markers (e.g., syntenin-1, TSG101) in the different types of EVs (Fig. S3D). Of

note, however, fewer large EVs pelleting at 2K and more medium-sized EVs at 10K were recovered, and consequently more specific association of CD63 with the 100K pellet, and more actinin-4 in the 10K pellet than in human DCs were observed (Fig. S3D). Thus, in EVs recovered from murine DCs and different human cell lines, several markers behave as they do in EVs from human DCs.

Separation of sEV Subtypes by Immuno-Isolation with Antitetraspanin Antibodies. Finally, to analyze the heterogeneity of the sEVs recovered in the 100K pellet of ultracentrifugation, we performed a final separation step by immuno-isolation using beads coated with antibodies targeting either CD9, CD63, or CD81 (Fig. 5A). To recover information not only on sEVs bearing these tetraspanins, but also on those devoid of them, we compared the pulled-down (PD) EVs with the EVs remaining in the flow-through (FT). Specificity of the immuno-isolation was verified using beads bearing an irrelevant antibody (IgG). Side-by-side comparison by Western blot (Fig. 5B) of the PD and FT performed with anti-CD9 beads showed that all CD9-, all CD63-, and all CD81-bearing EVs had been captured, but that abundant MHC II-bearing EVs had escaped capture and were detected in the FT. Therefore, the sEV pellet contains both CD9⁺ and CD9⁻ MHC II-bearing EVs. Upon capture by anti-CD63-coated beads, not only MHC II, but also clear CD9⁺ and some CD81⁺ signal remained in the FT, whereas CD81-coated beads isolated all of CD63, and almost all CD9 signal. These results suggest that CD63-bearing sEVs represent a subpopulation, which also bears the other tetraspanins, but that CD63⁻ EVs bearing CD9 or CD81 are also present. Full proteomic analysis of all these fractions was then performed and evidenced over 1,450 proteins, of which 700 were detected with at least three peptides in three biological replicates of at least one immuno-isolation (Fig. 5C and E and Dataset S3). Sixty-one of these proteins were also isolated by the irrelevant IgG-coated beads. In addition to sticky or very abundant proteins that are recovered nonspecifically in numerous immunoprecipitation (IP) experiments (crapome.org) (18)—such as cytoskeleton and heat-shock proteins, elongation factors, and histones—some of the F5-100K-enriched proteins were recovered in the IgG-PD: MVP, hornerin, complement C3, and serum albumin. Abundant presence of some transmembrane proteins [especially α M/ α X β 2 integrins (*ITGAM*, *ITGAX*, *ITGB2*) and CD45 (*PTPRC*)], suggests that these proteins are associated to a subpopulation of EVs able to bind IgG or protein A. These proteins were excluded from the rest of the analysis.

Efficacy of the immuno-isolation with each specific antibody was confirmed by the identification of each immuno-isolated tetraspanin in its PD, but not in the FT (Dataset S3). Fewer proteins were recovered in the FT of anti-CD9 (228), than anti-CD81 (476), and anti-CD63 (500). Conversely, fewer proteins were recovered in the PD of anti-CD63 (294), than anti-CD81 (373) and anti-CD9 (381), thus confirming that CD63 is present on a more restricted sEV subpopulation. Quantitative comparison of the PD proteins followed by PCA (Fig. 5D) also showed that CD63-PDs were distinct from both CD9- and CD81-PD. Fifty-one percent of proteins were PD by the three antibodies (241 of 469) (Fig. 5E). Of these common proteins, a majority (161) (Fig. 5E, Lower) was also identified in the FT of anti-CD9, and is thus common to all sEVs. Among our newly identified sEV-specific proteins, Annexin XI, EHD4, and ADAM10 belong to this category. In contrast, two of our sEV markers were specific to the tetraspanin-enriched sEVs: TSG101 and syntenin-1.

GO term analysis was performed to determine the intracellular origin of the different EVs. In all tetraspanin PD and all FT, the most significantly enriched terms were those associated to EVs (i.e., extracellular-exosome, -vesicle, -organelle). Proteins common to CD9-, CD63-, and CD81-PD and excluded from the FT (Fig. 5D, Lower) displayed significant enrichment of several endosome-related terms (endosome, endocytic, phagocytic, and so on), with

P values lower than 10^{-5} , whereas proteins found exclusively in the FT did not display endosome enrichment. These results suggest that the nontetraspanin-bearing EVs do not correspond to the original definition of exosomes (i.e., endosome-derived sEVs). Among the tetraspanin-enriched sEVs, the subpopulation bearing CD9 in the absence of CD63 and CD81 contained 64 specific proteins and displayed enrichment in PM and endocytic vesicle terms, but not in

other endosome terms (Fig. 5E). Integrin $\alpha 2B$ (*ITGA2B* or CD41) was specifically pulled down with CD9. This integrin was previously shown to be enriched in medium-sized EVs released by platelets (19). Therefore, the subpopulation of CD9-single positive sEVs probably forms at the PM and early endocytic locations.

Fig. 5F summarizes the respective association to EV subtypes of the major proteins analyzed here: these proteins were previously

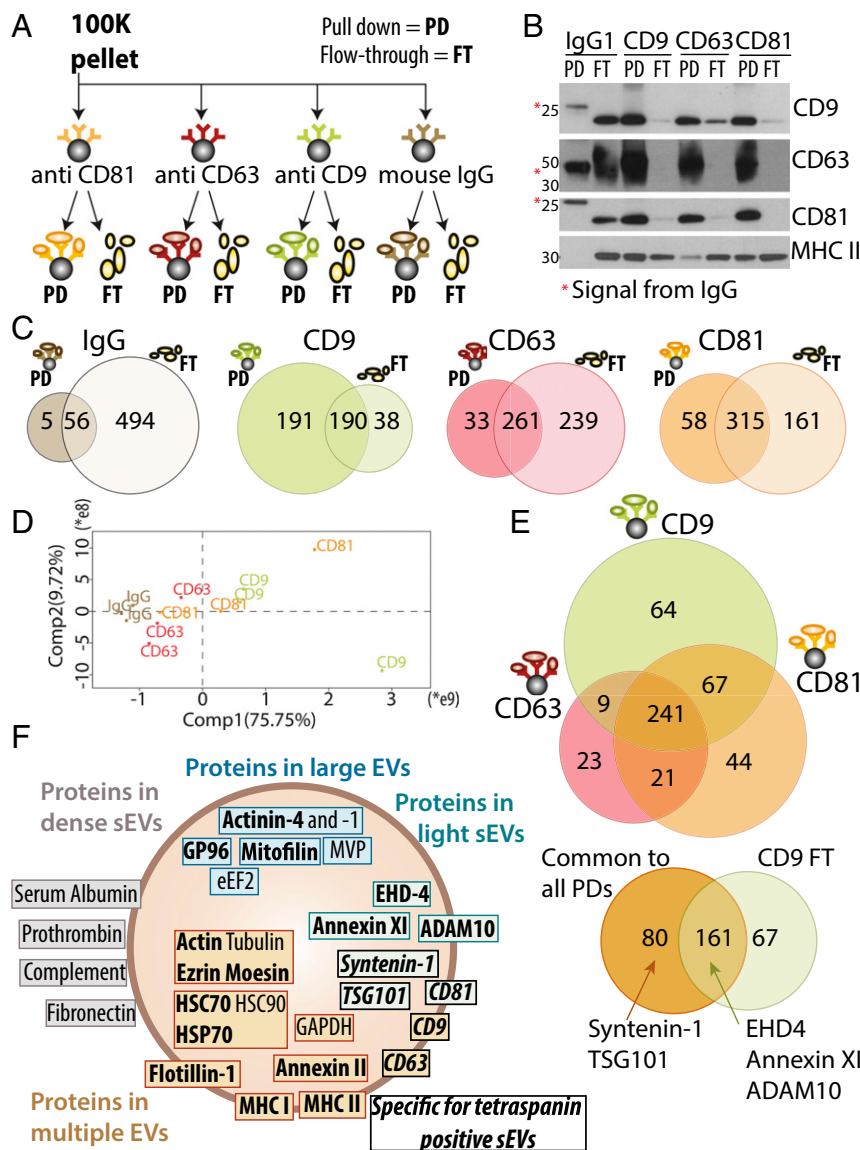


Fig. 5. Qualitative and quantitative proteomic analyses of sEVs immuno-isolated by CD9, CD63, or CD81-specific antibodies evidence additional sEV subpopulations. (A) The crude DC-derived 100K pellet was subjected to parallel immuno-isolation with beads coupled to irrelevant murine IgG, or antibodies against CD9, CD63, or CD81. PD vesicles and nonpulled down materials remaining in the FT were subjected to subsequent comparative analysis. (B) Equal volumes of materials from each PD and FT (the latter after concentration by ultracentrifugation) were loaded on a gel for Western blot analysis with antibodies specific for CD9, CD63, CD81, or MHC class II. All beads precipitated efficiently vesicles bearing the targeted protein. Note the remaining presence of CD9⁺ and CD81⁺ materials in the FT of CD63-beads, and of MHC II⁺ materials in the FT of all immuno-isolations, showing the existence of tetraspanin-negative sEVs. *Nonspecific signal from the immunoglobulins' heavy (50 kDa, CD63 blot) or light (25 kDa, CD9 and CD81 blots) chains used for immuno-precipitation. (C) PD and FT obtained as shown in A and B were analyzed by label-free LC-MS/MS. Venn diagrams represent the number of proteins detected in each sample with minimum three peptides in each of three independent replicates, comparing PD and FT obtained from each antibody after exclusion of the 61 proteins present in the PD of irrelevant IgG. (D) Quantitative PCA shows that the CD63-PD are distinct from the CD81- and CD9-PD. (E) Venn diagram showing proteins identified in PD obtained from the three antitetraspanin antibodies (Upper), and distribution of the 241 proteins common to the CD9-, CD63-, and CD81-PD, compared with the FT of CD9 (Lower). Position of sEV-specific proteins is indicated. (F) Assignment of the proteins analyzed here, and previously described as canonical exosome markers, to the different types of EVs, as demonstrated by Western blotting (bold) or by the quantitative proteomic comparison. EVs are schematized as a lipid bilayer (thick brown circle) enclosing cytosol (light background). Brown: proteins shared by several types of EVs. Green: proteins specifically enriched in F3-100K (i.e., the light sEVs), including those specific of the tetraspanin-enriched endosome-derived exosomes (italic font), and those ubiquitously present in all sEVs. Gray: proteins coisolated with the small EVs (100K pellets) but in EVs of higher density (F5-100K). Blue: proteins specifically enriched in large and medium-sized EVs.

described in sEVs (i.e., 100K pellets) secreted by mouse DCs (20) and other cells (21, 22), and listed by us as components of “canonical exosomes” (23), but our results now show that only a restricted subset of these proteins represent sEV-specific markers, among which a subfraction is associated to tetraspanin-enriched EVs corresponding to endosome-derived exosomes.

Discussion

The work presented herein provides: (i) two possible flow-charts for comprehensive analysis of mixed EVs, which we think should be performed initially on any given source of EVs: successive centrifugations followed by either floatation or parallel immunoprecipitation with three different tetraspanin-specific antibodies; (ii) a comprehensive comparative proteomic analysis of different subtypes of EVs of different sizes, densities, and tetraspanin composition secreted by a single cell type; and (iii) a confirmation, for some proteins identified by the above analysis, of their selective presence in one or the other subtype of EVs, coming from a variety of different cells.

Based on this analysis, we would like to propose the following categorization of EVs, which could be applied to any source of EVs, from cultured cells or from biological fluids: (i) large EVs pelleting at low speed, (ii) medium-sized EVs pelleting at intermediate speed, and (iii) sEVs pelleting at high speed. Among the sEVs, four subcategories can be defined: (iiia) sEVs coenriched in CD63, CD9, and CD81 tetraspanins and endosome markers (i.e., bona fide exosomes); (iiib) sEVs devoid of CD63 and CD81 but enriched in CD9 (associated with PM and an early endocytic signature); (iiic) sEVs devoid of CD63/CD9/CD81; and (iiid) sEVs enriched in ECM or serum-derived factors, the latter two categories not being associated to the endosomal pathway.

To distinguish these categories, we propose the concomitant use of the following combination of markers (summarized in Fig. 5F): (i) any cell membrane protein can be used to demonstrate the vesicular nature of the analyzed materials, for example MHC I and MHC II, which are present in all EVs of DCs; (ii) GP96 and possibly other ER-associated proteins are mainly present in large EVs; (iii) actinin-4 and mitofilin, and possibly other mitochondrial proteins, are present in both large and medium-sized EVs but absent from the sEVs; (iv) syntenin-1, TSG101, ADAM10, and EHD4 are only present in the sEVs, syntenin-1 and TSG101 being specific of the tetraspanin-enriched sEVs representing bona fide “exosomes”; and (v) ECM (collagen, PEDF = *SERPINF1*), complement (C3, C4A), and serum-derived factors (prothrombin, serum albumin) represent sEV-bound components of variable presence.

The fifth group of markers contains the proteins we observed specifically enriched in the F5-100K fraction and underrepresented in the 10K fractions and immuno-isolated by a non-specific IgG (Fig. 3D, Table S1, and Datasets S2 and S3). This list includes various keratins (classically considered contaminants of proteomic analyses), collagen (*C04A*), fibronectin, an ECM protein previously described in trophoblast or tumor cell-derived exosomes (17, 24), and hornerin, a S100 family member also found in the ECM of breast tumors (25). In addition, Complement (C3 and C4A), PEDF and prothrombin (F2), probably come from the serum used for culture and associate extracellularly with EVs after their secretion. The molecular mechanisms leading to association of such proteins to sEVs need further investigations, but our observations suggest that ECM and coagulation/complement proteins represent a particular category of sEV-associated components.

A major result of our work is that some proteins often used as “exosome markers,” such as MHC class II or class I molecules, heat-shock proteins 70 (constitutive HSC70/HSP73 and inducible HSP70/HSP72), flotillins, or actin, are present in all types of EVs, and thus cannot be considered as either exosome- or even sEV-specific markers (Fig. 1 and Fig. S1). We propose, however, newly validated sEV-specific, and among them exosome-specific,

proteins to be used as markers. To obtain these results, it was necessary to combine several separation procedures and to follow a nonbiased approach, rather than a molecule- or EV subtype-targeted one. Some groups have recently performed comparative proteomic analyses of medium-sized and small EVs (with or without floatation into a gradient) from platelets (19) or tumor cells (26–29). Another group has compared the expression of a few surface proteins on B lymphoma-EVs immunoprecipitated with either CD9, CD63, or CD81 (30). Our results are consistent with these other recent works, especially in identifying sEV-enriched proteins (e.g., TSG101 and CD81). However, our comparison of several additional subtypes of EVs leads to a higher refinement of definitions. We took advantage of an interesting observation that short-term floatation (i.e., upward displacement) into iodixanol gradients allows separation of discrete EV subtypes pelleted at the same speed but displaying different buoyant densities (Fig. 2B). Of note, however, this floatation protocol would not separate medium and small EVs if they had not been first separated by another means (here: centrifugation). In contrast, a sucrose gradient separated the medium and small EVs in two adjacent fractions of slightly different densities (respectively 1.17 and 1.15 g/mL) (Fig. 2D). Thus, heterogeneous EVs would have been separated with this approach, but with too much overlap and potential mixing to allow clear-cut differentiation by proteomic quantitation.

In addition to these gradient-mediated separations, sEV immuno-isolations with the three tetraspanins, and their comparative proteomic analysis with the remaining sEVs escaping PD demonstrated that some protein markers are really unique to a subclass of sEVs, whereas some others are generic. In particular, Annexin XI (but also Annexins V and VI) (Dataset S3), ADAM10, ACE, and EHD4 are present in all sEVs. Flotillins were also found in all sEVs, bearing or not tetraspanins, which probably explains why they were recovered in different sucrose gradient fractions than CD63 in tumor-derived EVs (31). The GO term enrichment analysis and the identity of proteins found in the tetraspanin-bearing sEVs confirm their relationship with the endosomal pathway, but also that sEVs can originate along different stages of this pathway. For example, tetraspanin-sEV-specific markers include syntenin-1 [involved in receptor targeting to intraluminal vesicles of MVBs (31)] and some of the endosomal sorting complex required for transport (ESCRT) proteins, TSG101, CHMP4A-B, and VPS4B (Fig. 5E and Dataset S3). Interestingly other ESCRT- or endosome-associated proteins [e.g., ALIX (*PDC61P*) and EHD1] are fully coimmunoprecipitated with CD9, but not with CD63 and CD81, suggesting that formation of some CD9-bearing sEVs involves a fraction of the endosomal machinery. Presence of some specific transmembrane proteins in the CD9⁺ sEVs (e.g., integrin α 2B, matrix metalloproteinase MMP14) (Dataset S3) will allow researchers to specifically isolate this subtype in the future.

Given the more restricted set of sEVs captured via CD63, and the general enrichment of CD63 in late endosomes (32), it is tempting to propose anti-CD63 as the preferred approach to isolate endosome-derived exosomes among the sEVs. Some cell types, however, secrete sEVs devoid of CD63 (30, 33, 34), and for these it will be necessary to analyze instead either CD81- or CD9-bearing sEVs. In addition, given its presence in large EVs, CD63 cannot be used as specific exosome-isolation tool without a first step of elimination of these large EVs.

Finally, our results will also provide leads to identify specific markers of the medium-sized EVs, which probably correspond to large oncosomes described in some tumor cells (27, 35, 36). We show here that actinin-4 is abundant in medium-EVs, and underrepresented in sEVs. The group of Di Vizio proposed to use cytokeratin 18 (*KRT18*) as a marker of oncosomes (27): it may be a specific marker of tumor-derived medium size-EVs, because we did not observe this keratin enriched in our proteomic analysis.

Furthermore, given the known classic nonspecific identification of keratins in all proteomic studies, we preferred not to focus on these molecules. Comparing the molecular signatures of tumor (26–29) and DC-derived (our work) medium EVs will surely provide additional specific markers. So far, we have not identified a protein that would be exclusively in medium EVs, and not also in the largest ones, which the other groups working on tumor-derived EVs did not evaluate: although it would be very useful, finding a specific marker for these particular EVs may be challenging.

The knowledge we provide herein, of which proteins to use as markers of different EV subtypes, will now be crucial to investigate the specific molecular machineries required for their biogenesis and secretion. These future studies will allow obtaining tools for selective inhibition or promotion of secretion each type of EV, a necessary approach to understand their physiological and pathological functions *in vivo*. Although several intracellular proteins (e.g., of the RAB, ESCRT, or SNARE families) have already been described as required for “exosome” biogenesis and secretion (reviewed in ref. 7), the effect of these machineries on secretion of the other EV subtypes was in most cases not investigated. We propose that any new drug, gene-inhibiting tool, or treatment claiming specific effects on a population of secreted EVs (especially on exosomes) should be systematically tested for its effects on other EVs. These investigations will crucially benefit from the knowledge of which specific protein markers to analyze, provided by our work.

Generation of these comprehensive maps of EV subtypes and their biogenesis/secretion machineries, together with new ongoing developments of techniques and protocols, will be crucial to unravel the complexity of the EV (and non-EV) network of circulating components present in biological fluids, and their respective value as biomarkers or therapeutic tools.

Materials and Methods

Cells. Monocyte-derived DCs were obtained from blood samples of healthy human donors as described in ref. 13. This study was conducted according to the Helsinki Declaration, with informed consent obtained from the blood donors, as requested by our Institutional Review Board. Peripheral blood mononuclear cells were purified by density gradient centrifugation (LymphoPrep, Axis Shield). CD14⁺ cells were enriched by magnetic sorting (Miltenyi Biotec) and cultured at 1–2 million cells per mL for 5 d in RPMI 1640 (Gibco) supplemented with 10% FCS (Biowest), 50 μ M 2-ME, 10 mM Hepes, 100 IU/mL penicillin and 100 μ g/mL streptomycin (Gibco) in the presence of IL-4 and GM-CSF (50 ng/mL and 100 ng/mL, respectively; Miltenyi Biotec). Cell lines HEK293T, RPE-1 (37), HeLa-CITTA (32), MDA-MB-231, SHIN, IGROV-1 (38), and OV2008 were cultured in DMEM-glutamax (or RPMI-glutamax for IGROV-1) supplemented with 10% FCS (Lonza), 100 IU/mL penicillin, and 100 μ g/mL streptomycin (Gibco).

Reagents. Antibodies for Western blot were: mouse monoclonal anti-human CD63 (clone H5C6, BD Biosciences), CD9 (clone CBL162, Millipore), CD81 (clone B-11, Santa-Cruz), flotillin-1 (clone 18/Flotillin-1, BD Biosciences), MHC class II [1B5 hybridoma anti-DR α (39)], actin (clone c4, Millipore), ADAM10 (clone #163003, R&D Systems), HSP70 (clone C92F3A-5, Enzo Life Science), MHC class I [HC10 (40) + HCA2 (41) hybridomas], anti-TSG101 (clone 51/TSG101, BD Biosciences); polyclonal mouse anti-human ALIX (Abnova); rat monoclonal anti-human HSC70 (clone 1B5, Enzo Life Sciences), and GP96 (clone 9G10, Enzo Life Sciences); rabbit polyclonal anti-human Annexin II (Genetex), Annexin XI (Genetex), actinin-4 (Genetex), mitofilin (Pierce Antibodies), EHD4 (gift from Steve Caplan, National Institutes of Health, Bethesda), and syntenin-1 (gift from Pascale Zimmerman, Centre de Recherche en Cancérologie de Marseille, France, or rabbit monoclonal clone EPR8102, Abcam); rabbit monoclonal anti-human LAMP2 [rabbit, clone EPR4207 (2), Genetex]. HRP-coupled secondary antibodies were purchased from Jackson Immuno-Research. Ultrapure Sucrose and iodixanol (Optiprep) were from Sigma. Lipid staining was performed with FM 4-64 FX dye (Life Technology): briefly cells were seeded on poly-L-lysine-coated glass coverslips overnight, placed on ice, stained for 5 min, and then fixed with ice-cold formaldehyde 4% (Electron Microscopy Sciences).

EV Isolation. Bovine EV-depleted medium was obtained by overnight ultracentrifugation at 100,000 \times g in a 45Ti rotor, of medium supplemented with 20% FCS. On day 5 of culture (DCs) or when subconfluence was reached (cell lines), cells were washed in PBS (Gibco) and further cultured in EV-depleted medium (10% EV-depleted FCS final) or in DMEM-Glutamax without FCS (MDA-MB-231 exposed to starvation) for 24 h before collection of conditioned medium for EV isolation. EVs were isolated by differential ultracentrifugation as previously described (11) (Fig. 1A). Briefly, conditioned medium was centrifuged at 300 \times g for 10 min at 4 $^{\circ}$ C to pellet cells. Supernatant was centrifuged at 2,000 \times g for 20 min at 4 $^{\circ}$ C (2K pellet), transferred to new tubes, and centrifuged in a 45Ti rotor (Beckman) for 40 min at 10,000 \times g (9,000 rpm = 10K pellet), and finally for 90 min at 100,000 \times g (30,000 rpm = 100K pellet). All pellets were washed in 50–60 mL of PBS and recentrifuged at the same speed before being resuspended in 50–100 μ L of sterile PBS. Cells recovered from the first 300 \times g pellet were pooled with cells detached from the plates by incubation at 4 $^{\circ}$ C in PBS-EDTA (DCs) or in trypsin-EDTA (adherent cells) (Gibco) and counted by Countess (Invitrogen). Viability was assessed by Trypan Blue stain 0.4% (Life Technologies) exclusion.

Iodixanol/Optiprep Gradient Separation. For iodixanol gradient separation, pellets obtained by ultracentrifugation from 80 to 200 million DCs were washed and resuspended in 1.5 mL buffer containing: 0.25 M sucrose, 10 mM Tris pH 8.0, 1 mM EDTA (pH 7.4), transferred to a SW55Ti rotor tube (Beckman), and mixed 1:1 with 60% (wt/vol) stock solution of iodixanol/Optiprep. A 40% iodixanol working solution was prepared [40% (wt/vol) iodixanol, 0.25 M sucrose, 10 mM Tris pH 8.0, 1 mM EDTA, final pH set to 7.4] and used to prepare 20% and 10% (wt/vol) iodixanol solutions. Next, 1.3 mL 20% (wt/vol) iodixanol and 1.2 mL 10% iodixanol were successively layered on top of the vesicle suspension and tubes were centrifuged for 1 h at 4 $^{\circ}$ C at 350,000 \times g (54,000 rpm) in SW55Ti (stopping without break); 10 fractions of 490 μ L were collected from the top of the tube. Density was assessed with a refractometer (Carl Zeiss). Fractions were diluted with 2.5 mL PBS and centrifuged for 30 min at 100,000 \times g (43,000 rpm) in a TLA 110 rotor (Beckman, Optima TL100 centrifuge). These concentrated fractions were resuspended in 30 μ L of PBS.

Sucrose Gradient Separation. Sucrose gradients were built manually as described in ref. 42. Briefly 2.0 M and 0.4 M sucrose solution in PBS were used to prepare 15 fractions with sucrose molarity ranging from 0.4 to 2.0 M. Pellets mixed with 2.5 M sucrose to 1.5 mL total volume were loaded at the bottom of a SW40Ti tube and the gradient was layered by pouring sequentially 750 μ L of each of the 15 solutions (from 2 M to 0.4 M). Tubes were centrifuged for 16 h at 4 $^{\circ}$ C at 200,000 \times g (35,000 rpm). After stopping the centrifuge without breaks, 12 fractions of 1 mL were collected from the top of the tube. Density measurement and collection of the vesicle fractions were performed as described above.

Immuno-isolation. Antibodies for immuno-isolation [mouse monoclonal anti-human CD63 (clone H5C6, BD Biosciences), CD9 (cat. no. CBL162, Millipore), CD81 (cat. no. CBL579, Millipore), and normal mouse polyclonal IgG (cat. no. 12-371, Millipore)] in a ratio of 1 μ g of antibody per 100 μ L of beads were coupled by overnight incubation at 4 $^{\circ}$ C to Pierce Protein A Magnetic Beads (Life Technologies). Beads were then washed three times with 500 μ L of PBS-0.001% Tween, resuspended in 500 μ L of the same buffer, to which sEVs from 15 million DCs in 25 μ L PBS were added, followed by overnight incubation at 4 $^{\circ}$ C with rotation. Bead-bound EVs were collected and washed three times in 500 μ L PBS-Tween. Nonbead-bound supernatant was pooled with the supernatants of bead washes and centrifuged for 30 min at 100,000 \times g (43,000 rpm) in a TLA 110 rotor (Beckman, Optima TL100 centrifuge), to generate concentrated FT. FT and bead-bound EV samples were resuspended in 30 μ L of loading buffer 1 \times (Invitrogen) and boiled at 95 $^{\circ}$ C for 5 min before loading on gel.

Western Blotting. Cells were lysed in 50 mM Tris, pH 7.5, 0.3 M NaCl, 0.5% Triton X-100, 0.1% sodium azide with a mixture of antiproteases (Roche) at a concentration of 4 \times 10⁶ cells in 100 μ L of buffer for 20 min on ice, then centrifuged at 18,500 \times g for 15 min. The pellet was discarded and the supernatant was kept for further analysis. Protein concentration was measured using Micro-BCA (Thermo Scientific) for both cell lysates and vesicle preparation in the presence of 0.2% SDS. Equivalent micrograms of proteins (Figs. 1 and 4 B and C and Fig. S1D), or pellets recovered from a given number of cells [i.e., a given volume of conditioned medium] (Figs. 4D and 5B and Fig. S3 B and D) were loaded for all samples from each preparation and analyzed simultaneously on NuPAGE 4–12% BisTris gels (Invitrogen). Materials secreted by 7.5 \times 10⁶ (Fig. 5B), or 10–25 \times 10⁶ cells (Fig. 4D and Fig. S3 B and D) was analyzed. Separation was performed under nonreducing

conditions. After transfer to Immobilon membranes (Millipore), antibody incubations and development were performed using BM Chemiluminescence Western blotting Substrate (POD) (Roche), and radiographic films (GE Healthcare and Thermo Scientific) (Figs. 1, 2, 4, and 5B, and Figs. S1D and S3 B and D) or a ChemiDoc Touch imager (Bio-Rad) (Fig. 4D, Right) were used for membrane exposure. Intensity of the bands was quantified using ImageJ software.

Nanoparticle Tracking Analysis. A LM10 Nanoparticle Tracking Analysis device (Malvern) was used according to ref. 43. Before each session, the size and concentration of standard silica beads (silica microspheres, 0.15 μm ; Polysciences) was measured. All settings for the camera were determined using the bead solution and fixed for all measurements during the session [camera level 8, camera shutter 3.73–8.75 ms (depending on the set of measurements), camera gain 250.00]. For each sample, at least five videos of 30–60 s with more than 200 detected tracks per video, and in at least one dilution, were taken and analyzed using the Nanoparticle Tracking Analysis software 2.3 with default settings. Results represent the mean of the videos at one dilution (Fig. S1B, Bottom) or all videos acquired for a given sample (Fig. S1B, Upper).

Electron Microscopy. Electron microscopy was performed on pellets stored at -80°C and never unfrozen. EV suspension in PBS was deposited on formvar-carbon-coated copper/palladium grids for whole-mount analysis as described previously (11, 13, 44). In case of double immunostaining, samples on grids were successively incubated with mouse anti-CD63, 15-nm protein-A-gold, 1% glutaraldehyde (Electron Microscopy Sciences), anti-MHC II, 10-nm protein-A-gold, and glutaraldehyde, and afterward contrasted and embedded in a mixture of methylcellulose and uranyl acetate. Vesicle size was assessed with ITEM analysis software (Soft Imaging Systems) or ImageJ software.

Proteomics and Mass Spectrometry Analysis. Three independent sets of iodixanol fractions recovered from 4.4×10^8 (two sets) or 2.8×10^8 cells pooled from two to three donors were simultaneously separated by SDS/PAGE and stained with colloidal blue (LabSafe Gel Blue GBiosciences). Three gel slices were excised per fraction for each set. For immuno-isolated samples and their flow-through (materials recovered from 1.5×10^7 cells), SDS/PAGE was used without separation as a clean-up step, and only one gel slice was excised. Subsequently, gel slices were washed and proteins were reduced with 10 mM DTT before alkylation with 55 mM iodoacetamide. After washing and shrinking the gel pieces with 100% (vol/vol) MeCN, we performed in-gel digestion using trypsin (Roche) overnight in 25 mM NH_4HCO_3 at 30°C . Peptides were analyzed by LC-MS/MS using an Ultimate 3000 system (Dionex) coupled to an LTQ-Orbitrap XL mass spectrometer (Thermo Fisher Scientific). Proteins were denatured, reduced, alkylated and digested with trypsin as described previously (45, 46) or trypsin/LysC. A nanoflow HPLC instrument (Ultimate 3000, Dionex) was coupled on-line to the LTQ-Orbitrap XL Hybrid Ion Trap-Orbitrap mass spectrometer (Thermo Scientific) and an RSLCnano system (Ultimate 3000, Thermo Scientific) to the Orbitrap Fusion Tribrid mass spectrometer (Thermo Scientific). Peptides were loaded onto a C18-reversed phase column (300- μm inner diameter \times 5 mm; Dionex), separated and MS data acquired using Xcalibur software. Peptides were separated by HPLC over a two-step gradient of 157 min from 0% to 30% (vol/vol) acetonitrile and of 20 min [from 30% to 50% (vol/vol)] and by UHPLC over a two-step gradient of 100 min [from 5% to 35% (vol/vol)] and of 15 min from 35% to 75% (vol/vol) acetonitrile (75- μm inner diameter \times 50 cm; C18 Pep-Map, Dionex) and analyzed in the Orbitrap XL or Orbitrap Fusion mass spectrometer (Thermo Scientific). Full-scan MS was acquired with 60,000 and

120,000 resolution in the Orbitrap analyzer, respectively and ions from each full scan were fragmented with CID or HCD, respectively and analyzed in the linear ion trap.

Mass Spectrometry Data Processing and Statistical Analysis. For identification, the data were searched against the UniProtKB-SwissProt human database using Mascot 2.3 (Matrix Science) through Proteome Discoverer 1.4 (Thermo Scientific) workflow editor tool. Enzyme specificity was set to trypsin and a maximum of two miscleavages was allowed. Oxidized methionine, N-terminal acetylation, and carbamidomethyl cysteine were set as variable modifications. Maximum allowed mass deviation was set initially to 2 ppm for monoisotopic precursor ions and 0.5 Da for MS/MS peaks.

All peptide/protein identification data were processed using the Institut Curie-developed software myProMS (myproms-demo.curie.fr) (47) v3.0 (work in progress), which performs search engine results validation, false-positive rate (FDR)-based data filtering, protein quantification, statistical analysis, and data visualization. FDR calculation uses the quality algorithm (48) and was set to 1% at the peptide level for the whole study. For qualitative analysis, a protein was considered present in an iodixanol fraction if identified by at least three distinct peptides in the group of three gel slices obtained per fraction, for at least one donor. For qualitative analysis of immuno-isolated samples, a protein was considered present if at least three peptides in all three donors were detected.

For label-free quantification, peptide XICs (Extracted Ion Chromatograms) were computed with MassChroQ v1.2.1 (49) using OBI-Warp alignment algorithm. A scale normalization was applied on the total signal to correct the XICs for each biological replicate as described by ref. 50. Protein ratios were computed as the geometrical mean of related peptides. To estimate ratio significance, a two-tailed t test was performed with a Benjamini–Hochberg FDR control threshold set to 0.05.

To assess replicate reproducibility for all fractions, PCA was performed using peptide XICs of common peptides in all subfractions replicates using ade4 package (51), based on R. GO enrichment analysis was performed as described by refs. 52 and 53.

Raw data have been deposited in the ProteomeXchange Consortium (www.proteomexchange.org) (54) via the PRIDE partner repository with dataset identifier PXD003257, and will be available in VesiclePedia (www.microvesicles.org) and EVpedia (student4.postech.ac.kr/evpedia2_xe/).

Statistical Analysis. Statistical analyses of Western blot and cell viability assays were performed using GraphPad Prism 6. Paired nonparametric (Wilcoxon signed-rank test) (Fig. 2B and Fig. S1C) or parametric (Student's t test) (Fig. S3A) tests were used to compare the different pellets obtained from DCs of each donor.

ACKNOWLEDGMENTS. We thank Dr. Pascale Zimmermann (Centre de Recherche en Cancérologie de Marseille and University Leuven) and Dr. Steve Caplan (National Institutes of Health) for generous gifts of antibodies; Drs. Patrycja Kozik and Christel Goudot for helpful discussions on proteomic analyses; Alan Guichard for help in fluorescence microscopy experiments; and Drs. Elodie Segura, Claire Hivroz, Nicolas Manel, and Sebastian Amigorena for critical reading of the manuscript. This work was supported by the French National Research Agency through the “Investments for the Future” program (France-BioImaging, ANR-10-INSB-04); the IDEX and Labex programs (ANR-10-IDEX-0001-02 PSL* and ANR-11-LABX-0043); a Fondation ARC Grant SL220120605293 (to C.T.) and a postdoc grant (to M.T.); “Région Ile-de-France” and Fondation pour la Recherche Médicale grants (to D.L.); Centre d'Investigations Cliniques IGR-Curie 1428; INSERM; and Institut Curie, including a PhD grant (to J.K.).

- Yáñez-Mó M, et al. (2015) Biological properties of extracellular vesicles and their physiological functions. *J Extracell Vesicles* 4:27066.
- Colombo M, Raposo G, Théry C (2014) Biogenesis, secretion, and intercellular interactions of exosomes and other extracellular vesicles. *Annu Rev Cell Dev Biol* 30: 255–289.
- Raposo G, Stoorvogel W (2013) Extracellular vesicles: Exosomes, microvesicles, and friends. *J Cell Biol* 200(4):373–383.
- Buzas EI, György B, Nagy G, Falus A, Gay S (2014) Emerging role of extracellular vesicles in inflammatory diseases. *Nat Rev Rheumatol* 10(6):356–364.
- van der Pol E, Böing AN, Harrison P, Sturk A, Nieuwland R (2012) Classification, functions, and clinical relevance of extracellular vesicles. *Pharmacol Rev* 64(3):676–705.
- Melo SA, et al. (2015) Glypican-1 identifies cancer exosomes and detects early pancreatic cancer. *Nature* 523(7559):177–182.
- Kowal J, Tkach M, Théry C (2014) Biogenesis and secretion of exosomes. *Curr Opin Cell Biol* 29:116–125.
- Gould SJ, Raposo G (2013) As we wait: Coping with an imperfect nomenclature for extracellular vesicles. *J Extracell Vesicles* 2:20389.
- Kanada M, et al. (2015) Differential fates of biomolecules delivered to target cells via extracellular vesicles. *Proc Natl Acad Sci USA* 112(12):E1433–E1442.
- Sedlik C, et al. (2014) Different immunogenicity but similar antitumor efficacy of two DNA vaccines coding for an antigen secreted in different membrane vesicle-associated forms. *J Extracell Vesicles* 3:24646.
- Théry C, Amigorena S, Raposo G, Clayton A (2006) Isolation and characterization of exosomes from cell culture supernatants and biological fluids. *Curr Protoc Cell Biol* Chapter 3:Unit 3.22.
- Robbins PD, Morelli AE (2014) Regulation of immune responses by extracellular vesicles. *Nat Rev Immunol* 14(3):195–208.
- Colombo M, et al. (2013) Analysis of ESCRT functions in exosome biogenesis, composition and secretion highlights the heterogeneity of extracellular vesicles. *J Cell Sci* 126(Pt 24):5553–5565.
- Aalberts M, et al. (2012) Identification of distinct populations of prostatesomes that differentially express prostate stem cell antigen, annexin A1, and GLIPR2 in humans. *Biol Reprod* 86(3):82.
- Zonneveld MI, et al. (2014) Recovery of extracellular vesicles from human breast milk is influenced by sample collection and vesicle isolation procedures. *J Extracell Vesicles* 3:24215.

16. Li X, Donowitz M (2014) Fractionation of subcellular membrane vesicles of epithelial and non-epithelial cells by OptiPrep™ density gradient ultracentrifugation. *Methods Mol Biol* 1174:85–99.
17. Antonyak MA, et al. (2011) Cancer cell-derived microvesicles induce transformation by transferring tissue transglutaminase and fibronectin to recipient cells. *Proc Natl Acad Sci USA* 108(12):4852–4857.
18. Mellacheruvu D, et al. (2013) The CRAPome: A contaminant repository for affinity purification-mass spectrometry data. *Nat Methods* 10(8):730–736.
19. Aatonen MT, et al. (2014) Isolation and characterization of platelet-derived extracellular vesicles. *J Extracell Vesicles* 3:24692.
20. Segura E, et al. (2005) ICAM-1 on exosomes from mature dendritic cells is critical for efficient naive T-cell priming. *Blood* 106(1):216–223.
21. Kalra H, et al. (2012) Vesiclepedia: A compendium for extracellular vesicles with continuous community annotation. *PLoS Biol* 10(12):e1001450.
22. Kim DK, et al. (2013) EVpedia: An integrated database of high-throughput data for systemic analyses of extracellular vesicles. *J Extracell Vesicles* 2:20384.
23. Chaput N, Théry C (2011) Exosomes: Immune properties and potential clinical implementations. *Semin Immunopathol* 33(5):419–440.
24. Atay S, Gercel-Taylor C, Taylor DD (2011) Human trophoblast-derived exosomal fibronectin induces pro-inflammatory IL-1 β production by macrophages. *Am J Reprod Immunol* 66(4):259–269.
25. Fleming JM, Ginsburg E, Oliver SD, Goldsmith P, Vonderhaar BK (2012) Hornerin, an S100 family protein, is functional in breast cells and aberrantly expressed in breast cancer. *BMC Cancer* 12:266.
26. Keerthikumar S, et al. (2015) Proteogenomic analysis reveals exosomes are more oncogenic than ectosomes. *Oncotarget* 6(17):15375–15396.
27. Minciacchi VR, et al. (2015) Large oncosomes contain distinct protein cargo and represent a separate functional class of tumor-derived extracellular vesicles. *Oncotarget* 6(13):11327–11341.
28. Xu R, Greening DW, Rai A, Ji H, Simpson RJ (2015) Highly-purified exosomes and shed microvesicles isolated from the human colon cancer cell line LIM1863 by sequential centrifugal ultrafiltration are biochemically and functionally distinct. *Methods* 87: 11–25.
29. Clark DJ, et al. (2015) Redefining the breast cancer exosome proteome by tandem mass tag quantitative proteomics and multivariate cluster analysis. *Anal Chem* 87(20): 10462–10469.
30. Oksvold MP, et al. (2014) Expression of B-cell surface antigens in subpopulations of exosomes released from B-cell lymphoma cells. *Clin Ther* 36(6):847–862.e1.
31. Baietti MF, et al. (2012) Syndecan-syntenin-ALIX regulates the biogenesis of exosomes. *Nat Cell Biol* 14(7):677–685.
32. Ostrowski M, et al. (2010) Rab27a and Rab27b control different steps of the exosome secretion pathway. *Nat Cell Biol* 12(1):19–30, 1–13.
33. Jakobsen KR, et al. (2015) Exosomal proteins as potential diagnostic markers in advanced non-small cell lung carcinoma. *J Extracell Vesicles* 4:26659.
34. Yoshioka Y, et al. (2013) Comparative marker analysis of extracellular vesicles in different human cancer types. *J Extracell Vesicles* 2:20424.
35. Muralidharan-Chari V, et al. (2009) ARF6-regulated shedding of tumor cell-derived plasma membrane microvesicles. *Curr Biol* 19(22):1875–1885.
36. Di Vizio D, et al. (2009) Oncosome formation in prostate cancer: Association with a region of frequent chromosomal deletion in metastatic disease. *Cancer Res* 69(13): 5601–5609.
37. Abrami L, et al. (2013) Hijacking multivesicular bodies enables long-term and exosome-mediated long-distance action of anthrax toxin. *Cell Reports* 5(4):986–996.
38. Tibaldi L, et al. (2013) New blocking antibodies impede adhesion, migration and survival of ovarian cancer cells, highlighting MFGE8 as a potential therapeutic target of human ovarian carcinoma. *PLoS One* 8(8):e72708.
39. Adams TE, Bodmer JG, Bodmer WF (1983) Production and characterization of monoclonal antibodies recognizing the alpha-chain subunits of human Ia alloantigens. *Immunology* 50(4):613–624.
40. Gauster M, Blaschitz A, Dohr G (2007) Monoclonal antibody HC10 does not bind HLA-G. *Rheumatology (Oxford)* 46(5):892–893, author reply 893–894.
41. Seitz C, Uchanska-Ziegler B, Zank A, Ziegler A (1998) The monoclonal antibody HCA2 recognises a broadly shared epitope on selected classical as well as several non-classical HLA class I molecules. *Mol Immunol* 35(13):819–827.
42. Bobrie A, Colombo M, Krumeich S, Raposo G, Théry C (2012) Diverse subpopulations of vesicles secreted by different intracellular mechanisms are present in exosome preparations obtained by differential ultracentrifugation. *J Extracell Vesicles* 1:18397.
43. Gardiner C, Ferreira YJ, Dragovic RA, Redman CW, Sargent IL (2013) Extracellular vesicle sizing and enumeration by nanoparticle tracking analysis. *J Extracell Vesicles* 2:19671.
44. Raposo G, et al. (1996) B lymphocytes secrete antigen-presenting vesicles. *J Exp Med* 183(3):1161–1172.
45. Lo Cicero A, et al. (2015) Exosomes released by keratinocytes modulate melanocyte pigmentation. *Nat Commun* 6:7506.
46. Burgo A, et al. (2013) Increased activity of the vesicular soluble N-ethylmaleimide-sensitive factor attachment protein receptor TI-VAMP/VAMP7 by tyrosine phosphorylation in the Longin domain. *J Biol Chem* 288(17):11960–11972.
47. Pouillet P, Carpentier S, Barillot E (2007) myProMS, a web server for management and validation of mass spectrometry-based proteomic data. *Proteomics* 7(15):2553–2556.
48. Käll L, Storey JD, Noble WS (2008) Non-parametric estimation of posterior error probabilities associated with peptides identified by tandem mass spectrometry. *Bioinformatics* 24(16):i42–i48.
49. Valot B, Langella O, Nano E, Zivy M (2011) MassChroQ: A versatile tool for mass spectrometry quantification. *Proteomics* 11(17):3572–3577.
50. Yang YH, et al. (2002) Normalization for cDNA microarray data: A robust composite method addressing single and multiple slide systematic variation. *Nucleic Acids Res* 30(4):e15.
51. Dray S, Dufour AB (2007) The ade4 package: Implementing the duality diagram for ecologists. *J Stat Softw* 22(4):1–20.
52. Pan C, Kumar C, Bohl S, Klingmueller U, Mann M (2009) Comparative proteomic phenotyping of cell lines and primary cells to assess preservation of cell type-specific functions. *Mol Cell Proteomics* 8(3):443–450.
53. Sury MD, Chen JX, Selbach M (2010) The SILAC fly allows for accurate protein quantification in vivo. *Mol Cell Proteomics* 9(10):2173–2183.
54. Vizcaino JA, et al. (2013) The PRoteomics IDentifications (PRIDE) database and associated tools: Status in 2013. *Nucleic Acids Res* 41(Database issue):D1063–D1069.
55. Théry C, et al. (1999) Molecular characterization of dendritic cell-derived exosomes. Selective accumulation of the heat shock protein hsc73. *J Cell Biol* 147(3):599–610.